

Marangoni Effect Reverses Coffee-Ring Depositions

Hua Hu^{*,†} and Ronald G. Larson

Department of Chemical Engineering, University of Michigan, Ann Arbor, Michigan 48109-2136

Received: February 13, 2006; In Final Form: March 9, 2006

We show here both experimentally and theoretically that the formation of “coffee-ring” deposits observed at the edge of drying water droplets requires not only a pinned contact line (Deegan et al. *Nature* **1997**, 389, 827) but also suppression of Marangoni flow. For simple organic fluids, deposition actually occurs preferentially at the center of the droplet, due to a recirculatory flow driven by surface-tension gradients produced by the latent heat of evaporation. The manipulation of this Marangoni flow in a drying droplet should allow one in principle to control and redirect evaporation-driven deposition and assembly of colloids and other materials.

Introduction

It is commonly observed that a drying droplet of coffee or dirty water leaves a ring, rather than a uniform spot, of solute deposits on a surface. More than a mere curiosity, this “coffee-ring” phenomenon and related effects are important in the deposition of DNA/RNA microarrays,^{1–3} spotting methods for gene mapping,⁴ drug discovery,⁷ and the manufacture of novel electronic and optical materials,^{5,6} including thin films and coatings.^{8–11} Deegan and co-workers^{12–14} first explained that the ring is produced because the contact line is pinned, and so solvent lost by evaporation at the droplet’s edge must be replaced by solvent drawn from the center of the droplet. The flow that brings fluid from the center to the edge of the droplet also carries solute, which is deposited in a ring at the edge as the solvent evaporates there; see Figure 1a. Deegan et al. supported this mechanism by an analysis of the height-averaged velocity field, and its effect on particle deposition, assuming rapid vertical diffusion of particles across the height of the droplet and adhesion of the particles onto the substrate. However, in this letter we show that this explanation is only part of the story and that in liquids with clean droplet surfaces in which evaporation induces thermal Marangoni flows the coffee-ring deposition is predominantly at the center rather than the edge of the droplet.

As a demonstration, we show in Figure 1b that fluorescent poly(methyl methacrylate) (PMMA) particles^{15,16} deposit preferentially near the center of a drying octane droplet. In Figure 1c, mica flakes also deposit near the center of the octane droplet as well as at the edge possibly because the disklike mica flakes are more easily collected at the wedge near the contact line than the spherical particles. Note that in our experiments with octane the glass coverslip was coated with perfluorolauric acid (PFLA) to produce a contact angle large enough to produce an observable Marangoni flow. In the following, we trace the difference between the deposition pattern in Figure 1a and that

in Figures 1b and 1c to a difference in the flow field in water versus octane droplets. In particular, we will show that in an octane droplet a Marangoni flow is generated due to a surface-tension gradient but that this flow, while theoretically expected for clean liquid surfaces, is suppressed in water droplets. Elsewhere,¹⁷ we computed numerically the evaporation-induced nonuniform cooling along the surface of a drying droplet. This cooling produces a temperature gradient that, in turn, leads to a surface-tension gradient along the droplet free surface. This surface-tension gradient, finally, induces a Marangoni (i.e., surface-tension-driven) flow that we here show carries particles that are near the free liquid surface of the droplet inward toward the top of the droplet and then plunges them downward where they can either adsorb onto the substrate near the center of the droplet or be carried along the substrate to the edge, where they are recirculated along the free surface back toward the top of the droplet. To obtain a quantitative theory for this Marangoni-reversed coffee-ring phenomenon, we here develop a fully analytical solution for the Marangoni flow in an evaporating droplet, use this in Brownian dynamics simulations of particle transport and deposition from the drying droplet, and compare predicted deposition patterns with patterns produced experimentally by drying water and octane droplets. Agreement between the experimental and predicted results is obtained for both the flow fields and the particle deposition patterns in the presence and in the absence of the Marangoni flow in the drying droplet.

Theory

Elsewhere,^{17,18} we demonstrated that momentum, mass, and heat transfer in the slowly evaporating droplet can be justified as quasi-steady processes in small, slowly drying droplets. Because of small capillary and bond numbers, the surface of the evaporating droplet with a pinned contact line can be regarded as a spherical cap. Since the particle concentration in the droplet is about 100–1000 ppm, which is very low, we neglect the effect of particles on fluid flow, thermal conductivity, and other physical-chemical properties of the solvent. Likewise, the number density of particles near the droplet free surface is

* Author to whom correspondence should be addressed. Email: hu.h.6@pg.com.

† Present address: The Procter & Gamble Company, 8256 Union Center Blvd., West Chester, OH 45069.

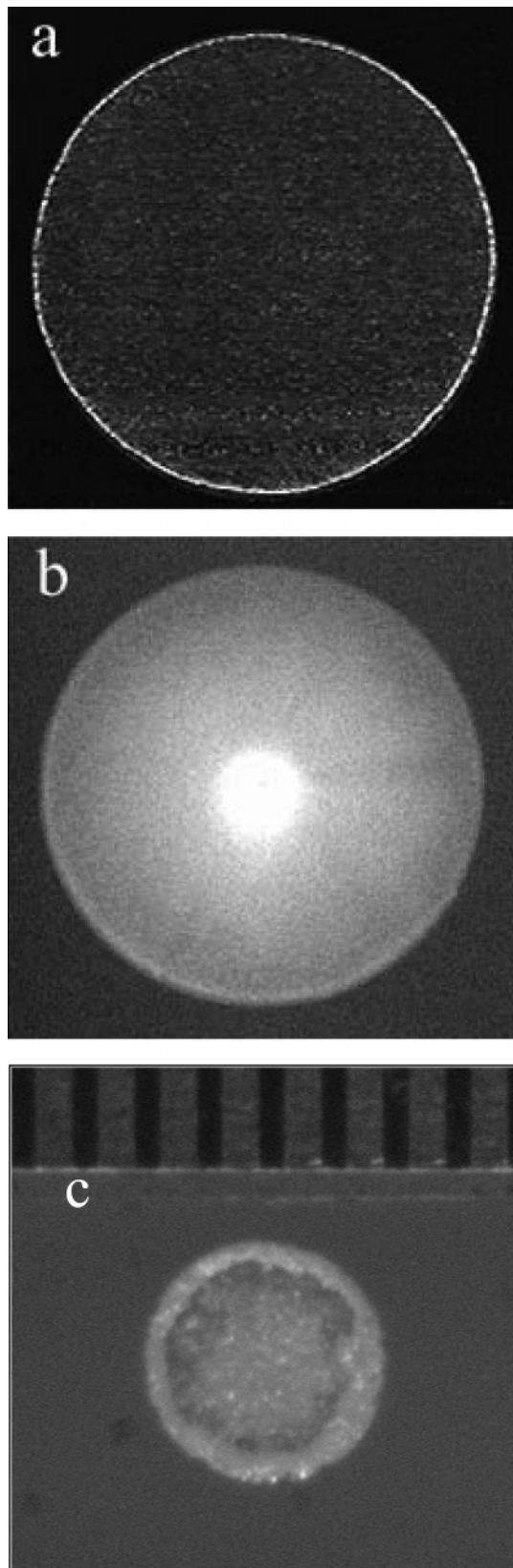


Figure 1. (a) Ring deposition pattern of fluorescent polystyrene particles (Molecular Probes, Inc.) deposited on a Corning No. 1 glass coverslip from a drying $0.5 \mu\text{L}$ water droplet containing $0.75 \mu\text{m}$ fluorescent particles (0.00025 g/mL), imaged using a Nikon inverted fluorescence microscope TE200. The excitation and emission wavelengths are 480 and 510 nm. (b) Deposition pattern from a $10 \mu\text{L}$ droplet of octane containing PMMA particles ($1 \text{ g}/100 \text{ mL}$) deposited on a glass coverslip coated with PFLA. (c) The same as part b except the particles are mica flakes (about $10\text{--}20 \mu\text{m}$, $0.1 \text{ wt } \%$). All experiments were performed at room temperature.

too small to create an appreciable osmotic pressure that might alter the droplet surface tension. Using lubrication theory, we earlier derived an approximate semianalytical solution for the flow field in the droplet in the presence or in the absence of Marangoni stress using a surface temperature profile obtained by finite element analysis of the heat transport equation. Here, however, we show that by neglecting the heat transfer in the radial direction because it is a second order in droplet flatness (the ratio of droplet height to contact line radius) we obtain an approximate analytical solution for the surface temperature T as a function of radial position r , namely

$$T - T_\infty = h_o H_v J(\tilde{r}, \theta) \sqrt{1 + \left(\frac{\partial \tilde{h}}{\partial \tilde{r}}\right)^2 \left(\frac{\tilde{h}}{k_1} + \frac{\tilde{h}_g}{k_2}\right)} \quad (1)$$

where T_∞ is the ambient temperature, H_v is the latent heat of evaporation of solvent, k_1 and k_2 are the thermal conductivities of the solvent and glass substrate, respectively, θ is the contact angle in units of radians, \tilde{h}_g is the dimensionless substrate thickness, $\tilde{h}_g \equiv h_g/h_o$, h_o is the initial droplet height, and \tilde{h} is the dimensionless droplet surface profile, which is given by

$$\tilde{h} \equiv \frac{h}{h_o} = \frac{R\sqrt{1/\sin^2 \theta - \tilde{r}^2} - R/\tan \theta}{h_o} \quad (2)$$

where R is the contact line radius and $\tilde{r} = r/R$ is the dimensionless radial position.

In eq 1, the surface evaporation flux J reported in our previous work is given by¹⁹

$$J(\tilde{r}, \theta) = J(0, \theta)(1 - \tilde{r}^2)^{-\lambda(\theta)} \quad (3)$$

$$J(0, \theta) = \frac{D(c_s - c_\infty)}{R} (0.27\theta^2 + 1.30)(0.6381 - 0.2239(\theta - \pi/4)^2) \quad (4)$$

where c_s and c_∞ are the vapor concentrations at the droplet surface and in the ambient air, respectively, D is the diffusivity of the vapor, and $\lambda(\theta)$ is a parameter reflecting the uniformity of evaporation flux along the droplet surface and is given by $\lambda(\theta) = 0.5 - \theta/\pi$.

With these analytical surface temperature and the evaporation flux distributions, we can derive a fully analytical solution for the temperature field (given above) and for the Marangoni flow field in the evaporating droplet whose contact line is pinned, namely

$$\tilde{u}_r = \frac{3}{8} \frac{1}{1 - \tilde{r}} \frac{1}{\tilde{r}} \left[(1 - \tilde{r}^2) - (1 - \tilde{r}^2)^{-\lambda(\theta)} \right] \left(\frac{\tilde{z}}{\tilde{h}^2} - 2 \frac{\tilde{z}}{\tilde{h}} \right) + \frac{\tilde{r} h_o^2 \tilde{h}}{R^2} (\tilde{J} \lambda(\theta) (1 - \tilde{r}^2)^{-\lambda(\theta)-1} + 1) \left(\frac{\tilde{z}}{\tilde{h}} - \frac{3}{2} \frac{\tilde{z}^2}{\tilde{h}^2} \right) + \frac{M a h_o \tilde{h}}{4R} \frac{d\tilde{T}}{d\tilde{r}} \left(2 \frac{\tilde{z}}{\tilde{h}} - 3 \frac{\tilde{z}^2}{\tilde{h}^2} \right) \quad (5)$$

$$\begin{aligned} \tilde{u}_z = & \frac{3}{4} \frac{1}{1-\tilde{t}} [1 + \lambda(\theta)(1-\tilde{r}^2)^{-\lambda(\theta)-1}] \left(\frac{\tilde{z}^3}{3\tilde{h}^2} - \frac{\tilde{z}^2}{\tilde{h}} \right) - \\ & \frac{3}{4} \frac{1}{1-\tilde{t}} [(1-\tilde{r}^2) - (1-\tilde{r}^2)^{-\lambda(\theta)}] \left(\frac{\tilde{z}^2}{2\tilde{h}^2} - \frac{\tilde{z}^3}{3\tilde{h}^3} \right) \frac{\partial \tilde{h}}{\tilde{r} \partial \tilde{r}} - \\ & \frac{h_o^2}{R^2} (\tilde{J} \lambda(\theta)(1-\tilde{r}^2)^{-\lambda(\theta)-1} + 1) \left(\tilde{z}^2 - \frac{\tilde{z}^3}{\tilde{h}} \right) - \\ & \frac{\tilde{r}^2 h_o^2}{R^2} \tilde{J} \lambda(\theta)(\lambda(\theta) + 1)(1-\tilde{r}^2)^{-\lambda(\theta)-2} \left(\tilde{z}^2 - \frac{\tilde{z}^3}{\tilde{h}} \right) - \\ & \frac{\tilde{r} h_o^2}{R^2} (\tilde{J} \lambda(\theta)(1-\tilde{r}^2)^{-\lambda(\theta)-1} + 1) \left(\frac{\tilde{z}^3}{\tilde{h}^2} \right) \frac{\partial \tilde{h}}{\partial \tilde{r}} - \\ & \frac{Ma h_o}{4R} \left(\tilde{z}^2 - \frac{\tilde{z}^3}{\tilde{h}} \right) \left(\frac{d^2 \tilde{T}}{d\tilde{r}^2} + \frac{1}{\tilde{r}} \frac{d\tilde{T}}{d\tilde{r}} \right) - \frac{Ma h_o}{4R} \left(\frac{\tilde{z}^3}{\tilde{h}^2} \right) \frac{d\tilde{T}}{d\tilde{r}} \frac{\partial \tilde{h}}{\partial \tilde{r}} \quad (6) \end{aligned}$$

where the dimensionless variables are given by $\tilde{u}_r = u_r t_f / R$, $\tilde{u}_z = u_z t_f / h_o$, $\tilde{t} = t / t_f$, $\tilde{z} = z / h_o$, $\tilde{J} \equiv J(0, \theta) / \rho \dot{h}$, $\tilde{h} = h_o / t_f$ and $\tilde{T} \equiv (T - T_c) / (T_e - T_c)$ and t_f is the drying time. T_e is the surface temperature at the edge of the droplet, T_c is the surface temperature at the top of the droplet, ρ is the density of solvent, Ma is the Marangoni number defined as $Ma \equiv -\beta(T_e - T_c) - t_f / \mu R$, β is the surface tension–temperature coefficient, and μ is the viscosity of the liquid. With the above fully analytical description of the flow (eqs 5 and 6), we can investigate its effect on particle deposition and compare these predictions to the experimental results that we now discuss.

Results and Discussion

For solvents such as octane and other alkanes that are not easily contaminated by surface-active agents, a strong recirculating flow is observed in the droplet—see Figure 2a—implying that a large Marangoni stress is generated along the droplet surface. In Figure 2a, we visualize the octane droplet from its side, so that the Marangoni flow is obvious. A 630 nm diode laser sheet with a thickness of 13 μm (much thinner than the droplet radius $R = 2$ mm) is used to illuminate the plane parallel to the central axis of the droplet. We use monodisperse 4.7 μm PMMA fluorescent particles as tracers to track the flow in the octane droplet. The PMMA particles, which are stable in alkane solvents and have long excitation and emission wavelengths of

645 and 670 nm, were specially synthesized in our lab.^{14,15} The PMMA particles were washed at least eight times by centrifugation with the HPLC-grade octane so that the PMMA particle suspension is free of any surfactants. Using classical geometrical optics, we corrected the effect of refraction due to the curved droplet interface on the observed flow field. Figure 2b is the theoretical flow field including the correction for the lens effect caused by refraction from the spherical-cap droplet. The theoretical streamlines agree well with the experimental ones. Using the experimental conditions (for octane, the contact-line radius R is 2 mm and $\beta = 0.0935$ dyn/(cm/K) and $\mu = 0.54$ cP), we can calculate that the Marangoni number is around 45800. Through the use of this value, the Marangoni velocity from our theory (eqs 1–6) in the region above the center of the vortex in the droplet ranges up to a maximum of 6.7 mm/s, while from the video clips available in the Supporting Information we find that the maximum experimental velocity in the same region is 7.2 mm/s. A complete measurement of the velocity field will be presented later. Note in Figure 2a the bright region near the substrate generated by the lens effect, which our theory also successfully predicts. During droplet evaporation, evaporative cooling reduces the droplet surface temperature nonuniformly. The temperature at the liquid–air surface at the top center of the droplet is the lowest due to a longer thermal conduction path, and the surface tension is highest there. This produces an inward flow near the droplet surface, whose shear stress balances the Marangoni stress, i.e., the surface-tension gradient.

For water droplets, Deegan et al. observed that the Marangoni flow is weak. We confirmed this finding using an out-of-focus particle tracking method, which depends on a precise optical relationship between the distance of a particle from the focal plane and the size of the out-of-focus particle image. In this way, by imaging in a focal plane, a three-dimensional particle displacement can be inferred for particles passing through that plane. We obtained the velocity at 47 different positions by tracking 15–20 particle trajectories at each position to minimize the Brownian-motion-induced white noise. Because the experiment is a transient one that only lasts a few minutes, gathering this many data points required the use of about 300 nearly identical droplets. Using this method, we measured the flow field in the evaporating water droplet; see the right half of the

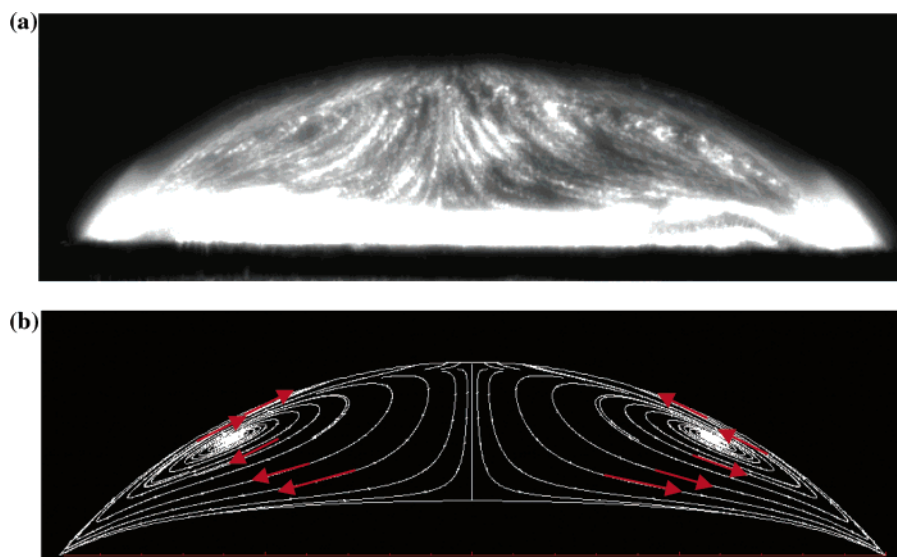


Figure 2. Flow field in a drying octane droplet, (a) imaged experimentally and (b) predicted ($Ma = 45\,800$). To observe a clear Marangoni vortex, the illumination plane was moved forward about 0.66 mm from the symmetrical axis of the droplet.

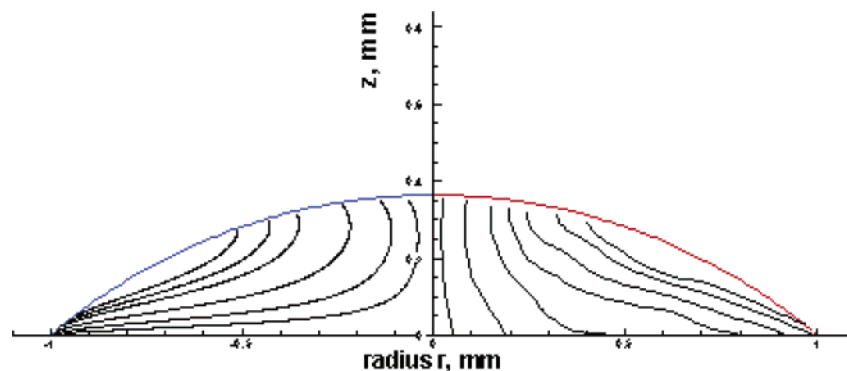


Figure 3. Streamlines in a drying water droplet, as measured (right half of droplet) and predicted (left half). The Marangoni number ($Ma = 8$) for the theoretical streamlines is obtained from a best fit to the experimental results.

droplet image in Figure 3. The experiments clearly show that the Marangoni flow is very weak in an evaporating water droplet. Although the theoretical Marangoni number for a drying water droplet is around $Ma = 1000$, the theoretical flow field shown on the left in Figure 2 can only be matched to the experimental one by lowering the Marangoni number 100-fold, to around $Ma = 8$. This huge reduction in apparent Marangoni number is evidently produced by surfactant contaminants.²⁰ In our experiments, we used the same particle system as that in the paper of Deegan et al. We also did our best by using double-distilled water and surfactant-free polystyrene particles to avoid introducing surfactants into the drying water droplet. However, like other authors,^{13,20} we found very weak Marangoni flows in water, much weaker than expected theoretically, and we attribute this to the well-known difficulty of keeping water surfaces sufficiently clear of contaminants. Including the effects of insoluble surfactants on the flow field, we can show¹⁷ that 100-fold reduction of the Marangoni strength is achieved with a concentration of surfactant contaminants as small as 300 molecules/ μm^2 .

The different flows in the water versus the octane droplet produce the different substrate deposition patterns in Figure 1, which we can explain through our fluid flow expressions, eqs 5 and 6. Convection dominates the deposition pattern since the time scale for a $0.75 \mu\text{m}$ particle to diffuse a distance equal to the height of the droplet, $360 \mu\text{m}$, is about 50 h, which is much longer than the few minutes needed to convect the particle across the droplet. This means that the assumption of Deegan et al. that rapid vertical redistribution of particles occurs over the height of the droplet is inappropriate. Hence, one cannot in general use a simple height-averaged velocity field to predict the deposition pattern of particles from a drying droplet. Since Marangoni flow superimposes a circulation on the base flow but does not affect the height-averaged flow, the assumption of rapid diffusion of particles across the droplet height would predict a deposition pattern that is not affected by Marangoni flow, in contrast to our observations. We can, however, account for the roles of both diffusion and three-dimensional convection in the particle deposition process by performing Brownian dynamics simulations of particle motion in the full flow field given by eqs 5 and 6. In our Brownian dynamics simulations the particles are considered to be simple spheres whose interactions with each other are neglected and that convect and diffuse in the flow field until they impact the substrate, where they are assumed to remain fixed in position. Figure 4 compares the particle deposition profiles measured and those predicted by the Brownian dynamics simulations, both with (Figures 4a and 4b) and without (Figures 4c and 4d) Marangoni flow in the drying droplet. In both cases, good agreement is found

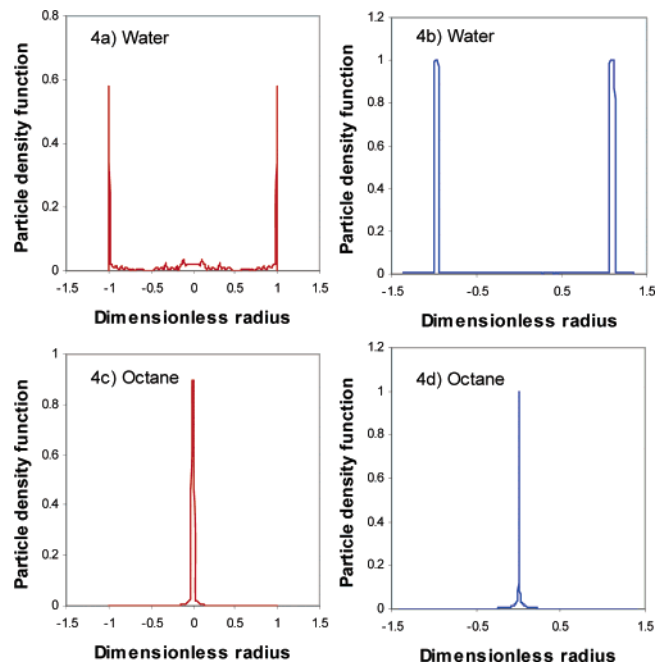


Figure 4. Normalized deposited particle density distribution for drying water (a and b) and octane droplets (c and d). Parts a and c are from experiments, and parts b and d from Brownian dynamics simulations using eqs 5 and 6. The experimental result is extracted from the light intensity distribution in Figure 1.

between experiments and simulations. The particle density profiles show a large peak at the center of the droplet when the Marangoni flow is strong. When Marangoni flow is weak or absent, only a small or no, peak is seen at the center, but a large peak is observed at the droplet's edge.

Our direct imaging of the flow in water and octane droplets leaves no doubt that the Marangoni flow in the water droplet is vastly weaker than that in the latter octane droplet. Although we have no direct proof that unintended surface-active agents in water are the cause, water is well-known to highly attract surface-active agents and therefore to rarely exhibit the surface tension of completely pure liquid water. The deposition patterns from the two fluid droplets are completely consistent with the observed flows, assuming irreversible deposition of particles. We note that there are numerous complexities in such flows that might affect the quantitative or even qualitative accuracy of our predictions, including imperfect particle adsorption to surfaces, surface roughness, inadvertent liquid heating caused by droplet illumination, as well as surfactant contamination. In addition, near the very end of drying, the particle concentration is high, the contact line breaks loose, and a thin film retreats

irregularly across the substrate. However, at least for the fluids and particles considered here, such issues seem not to be dominant ones, although they might have large effects in other situations.

Conclusions

In summary, our experimental and theoretical results now reveal that the coffee-ring phenomenon requires not only a pinned contact line, particles that adhere to the substrate, and high evaporation rate near the droplet's edge *but also that the Marangoni effect resulting from the latent heat of evaporation be suppressed*. For clean interfaces, free of surfactants, the Marangoni flow reverses the coffee-ring phenomenon and produces deposition at the droplet center rather than the edge. Our full analytical solution for the flow field, including Marangoni effects, agrees both with measurements of the flow field and with the observed deposition patterns, with both strong and weak Marangoni effects. Moreover, our results indicate that one could manipulate both the flow field and the deposition patterns by controlling temperature profiles through patterned heating of the substrate using resistive microheaters or through radiative heat transfer to the droplet surface. Our results both provide a more complete understanding of the coffee-ring phenomenon and suggest ways to better control drying droplet flows for biochemical assays and materials deposition.²¹

Acknowledgment. We thank the NASA microgravity research division for supporting this study through grants NAG3-2134 and NAG3-2708.

Supporting Information Available: Video clip showing Marangoni flow. The video clip was generated using Divx codec, which can be downloaded from <http://www.divx.com>.

This material is available free of charge via the Internet at <http://pubs.acs.org>.

References and Notes

- (1) Schena, M.; Shalon, D.; Davis, R. W.; Brown, P. O. *Science* **1995**, *270*, 467.
- (2) Schena, M.; Shalon, D.; Heller, R.; Davis, R. W.; Brown, P. O. *Proc. Natl. Acad. Sci. U.S.A.* **1996**, *93*, 10614.
- (3) Pirrung, M. C. *Angew. Chem., Int. Ed.* **2002**, *41*, 1276.
- (4) Jing, J.; Reed, J.; Huang, J.; Hu, X.; Clarke, V.; Edington, J.; Housman, D.; Anantharaman, T. S.; Huff, E. J.; Mishra, B.; Porter, B.; Shenker, A.; Wolfson, E.; Hiort, C.; Kantor, R.; Aston, C.; Schwartz, D. C. *Proc. Natl. Acad. Sci. U.S.A.* **1998**, *95*, 8046.
- (5) Kawase, T.; Siringhuas, H.; Friend, R. H.; Shimoda, T. *Adv. Mater.* **2001**, *13*, 1601.
- (6) Norris, D. J.; Arlinghaus, E. G.; Meng, L. L.; Heiny, R.; Scriven, L. E. *Adv. Mater.* **2004**, *16*, 1393.
- (7) Zhang, D. M.; Xie, Y.; Mrozek, M. F.; Ortiz, C.; Davisson, V. J.; Ben-Amotz, D. *Anal. Chem.* **2003**, *75*, 5703.
- (8) Chakrpani, N.; Wei, P. Q.; Carrillo, A.; Ajayan, P. M.; Kane, R. S. *Proc. Natl. Acad. Sci. U.S.A.* **2004**, *101*, 4009.
- (9) de Gans, B. J.; Duineveld, P. C.; Schubert, U. S. *Adv. Mater.* **2004**, *16*, 203.
- (10) Kimura, M.; Misner, M. J.; Xu, T.; Kim, S. H.; Russell, T. P. *Langmuir* **2004**, *19*, 9910.
- (11) Cawse, J. N.; Olson, D.; Chisholm, B. J.; Brennan, M.; Sun, T.; Flanagan, W.; Akhave, J.; Meharabi, A.; Saunders, D. *Prog. Org. Coat.* **2003**, *47*, 128.
- (12) Deegan, R. D.; Bakajin, O.; Dupont, T. F.; Huber, G.; Nagel, S. R.; Witten, T. A. *Nature* **1997**, *389*, 827.
- (13) Deegan, R. D.; Bakajin, O.; Dupont, T. F.; Huber, G.; Nagel, S. R.; Witten, T. A. *Phys. Rev. E* **2002**, *62*, 756.
- (14) Deegan, R. D. *Phys. Rev. E* **2000**, *61*, 475.
- (15) Hu, H.; Larson, R. G. *Langmuir* **2004**, *20*, 7436.
- (16) Hu, H.; Larson, R. G. *J. Am. Chem. Soc.* **2004**, *126*, 13894.
- (17) Hu, H.; Larson, R. G. *Langmuir* **2005**, *21*, 3972.
- (18) Hu, H.; Larson, R. G. *Langmuir* **2005**, *21*, 3963.
- (19) Hu, H.; Larson, R. G. *J. Phys. Chem. B* **2002**, *106*, 1334.
- (20) Savino, R.; Paterna, D.; Favaloro, N. *J. Thermophys. Heat Transfer* **2001**, *16*, 562.
- (21) Nguyen, V. X.; Stebe, K. J. *Phys. Rev. Lett.* **2002**, *22*, 3282.